



Evolution of boron-interstitial clusters in preamorphized silicon without the contribution of end-of-range defects

Maria Aboy^{a,*}, Lourdes Pelaz^a, Pedro López^a, E. Bruno^b, S. Mirabella^b, E. Napolitani^c

^a Campus Miguel Delibes, University of Valladolid, 47011 Valladolid, Spain

^b MATIS CNR-INFN Via Santa Sofia 64, I-95123 Catania, Italy

^c MATIS CNR-INFN at Dipartimento di Fisica, Via F. Marzolo 8, I-35131 Padova, Italy

ARTICLE INFO

Article history:

Received 5 May 2008

Received in revised form

11 September 2008

Accepted 16 September 2008

Keywords:

Modeling

Silicon

Defects

Activation

Diffusion

ABSTRACT

Kinetic Monte Carlo simulations have been used to investigate mechanisms for boron clustering in crystalline and preamorphized Si. We have extended previous boron-interstitial cluster models to include larger and more stable complexes in order to reproduce boron cluster evolution at very high boron concentrations. We have investigated the stoichiometry of boron-interstitial clusters resulting from low temperature recrystallization of preamorphized layers. We have performed a dedicated experiment based on boron implanted into preamorphized Si with end-of-range defects placed far enough from the boron profile to avoid the interaction between end-of-range defects and resulting boron-interstitial clusters after recrystallization. Hall measurements on active B dose combined with a systematic analysis performed by Kinetic Monte Carlo simulations indicate that initial boron-interstitial clusters after recrystallization should not contain a high amount of Si interstitials. Otherwise, boron deactivation and subsequent reactivation will occur faster than experimentally observed. The present results suggest B₃ and B₃I clusters as the most probable configurations after recrystallization.

© 2008 Elsevier B.V. All rights reserved.

1. Introduction

Boron implantation in Si is one of the most prevalent method to p-type dope semiconductor for junction formation. However, as-implanted ions are usually electrically non-active, and the lattice damage deteriorates the device performance [1]. A subsequent anneal of the Si substrate is necessary to permit dopant atoms to incorporate into substitutional sites and become electrically active, and to repair the lattice damage. At the same time, undesirable dopant diffusion and dopant clustering occur [1–2]. These phenomena pose severe difficulties to the achievement of low-resistivity ultra-shallow junctions, which determine the electrical characteristics of devices.

Mechanisms for B clustering in crystalline Si have been extensively analyzed in the literature and several models have been proposed, based on theoretical calculations [3–5] or inverse modeling over experimental data [6–7]. To our knowledge, current models for B clustering are based on the formation of complexes of B atoms and Si interstitials (BICs) that contain only few B atoms. However, recently some authors have detected quite large BICs by transmission electron microscopy (TEM) analyses [8–9]

under conditions of very high B concentrations. Moreover, experiments reported by De Salvador et al. [10] reveals the existence of two main kinetics paths for BICs dissolution, a faster dissolution and a slower one. They suggest that the usual small BICs are responsible for the faster dissolution path whereas large and more stable BICs would be responsible for the slower dissolution path. Therefore, current models need to be extended to include the possibility of growth into these large and more stable configurations of BICs.

The increasing demand for highly doped ultra-shallow junctions has extended the use of preamorphizing implants followed by low temperature solid phase epitaxial regrowth (SPER) [11]. During low temperature SPER B atoms are electrically activated up to concentrations typically around $1.5\text{--}3 \times 10^{20}$ B/cm³, with minimal diffusion, whereas B atoms remain inactive at higher B concentrations and immobilized in BICs that are transferred into crystalline Si after recrystallization [7,11]. Moreover, residual end-of-range (EOR) defects beyond the amorphous–crystalline interface may remain if the thermal budget is too low, which is known to degrade dopant activation and junction depth during subsequent temperature processing [7,11]. Although some authors have investigated B clustering during SPER by theoretical calculations and have proposed several stable configurations for these BICs [12], there are still some uncertainties about the configurations of BICs after recrystallization.

* Corresponding author. Tel.: +34 983423683x5504; fax: +34 983423675.
E-mail address: marabo@tel.uva.es (M. Aboy).

In this work we use Kinetic Monte Carlo (KMC) simulations [13] following the same scheme as is previous work [6–7,13–15]. We have extended the B clustering model to explain and predict grow into large and more stable than usual BICs under very high B concentration conditions. Furthermore, we investigate the stoichiometry of BICs resulting from SPER by comparing KMC simulations with different initial configurations for BICs after SPER with experimental data resulting from specifically designed experiments.

2. Dissolution kinetics of BICs in crystalline Si: a model for large BICs

Classical models for B clustering included complexes of B atoms and Si interstitials, B_nI_m , that contain only few atoms, up to four B atoms and four interstitial defects generally [3–7]. To account for recent experimental evidences of the formation of quite large BICs [8–10], we have extended our model by including BICs with more than four B atoms. Based on experimental evidences [9–10] we propose the existence of two different species of B clusters: small and less stable BICs that would lead to a faster BIC dissolution rate and large and more stable BICs that would lead to a slower BIC dissolution rate. Since these large BICs have been observed only in the presence of very high B concentrations (well above equilibrium solid solubility limit (s.l.)) we propose that B_5I_m clusters have high potential energy, with negative binding energy. Otherwise, small B clusters tend to grow into large configurations even in the presence of low B concentrations, contrary to experimental evidences [7,10]. This extended model is consistent with previous studies for low and middle B concentrations under very different experimental conditions [7]. Only in the presence of very high B concentrations, BICs could evolve towards B_nI_m configurations with $n > 5$, which have again low potential energy in the model according to experimental suggestions [9–10]. Furthermore, the activation energy for the emission of mobile interstitial B (B_i) from these large configurations ($n > 5$) is higher than for usual small configurations (up to $n = 4$). Thus, for large configurations we establish an activation energy for the emission of B_i from stable configurations around 4.5 eV [9–10] whereas for usual small BICs was around 3.7 eV [10]. This causes a slower dissolution rate when larger BICs are formed at high B concentrations.

In order to test the model including large BICs, we investigate the dissolution mechanisms of B clusters formed by Si ion implantation into samples with substitutional B at concentrations either below or above s.l. (at 815 °C s.l. $\sim 3.8 \times 10^{19}$ B/cm³ [16]), similar to experiments reported by De Salvador et al. [10]. For this purpose we have considered fully substitutional box-shaped B profiles at concentrations below s.l. (10^{19} B/cm³ B box, sample A) and well above s.l. (2×10^{20} B/cm³ B box, sample B) and at a depth of 220 nm. In both samples Si ions were implanted with 20 keV (projected range around 30 nm) at a nonamorphizing dose of 1×10^{14} ions/cm². Then, a rapid thermal annealing at 815 °C for 5 min was performed. Simulations show that this thermal process fully dissolves the implant-induced defects and injects Si interstitials towards the B box which interact with B atoms causing the formation of BICs. Later, we perform additional anneals at 900 °C in both samples in order to analyze the evolution of the clustered B dose. In Fig. 1(a) we represent reported experimental data [10] for the evolution of the clustered B dose during annealing at 900 °C along with our simulation results obtained with previous models in which BICs are not allowed to grow beyond four B atoms. As discussed in Ref. [10], experimental data show that BICs dissolution in sample A shows only a fast dissolution rate

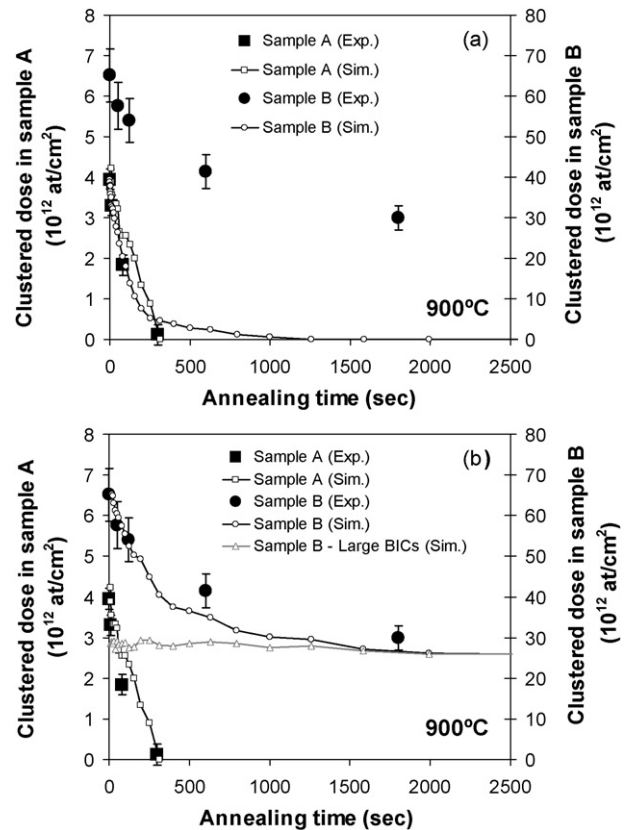


Fig. 1. Experimental data [10] and simulation results for the evolution of the clustered B dose as a function of annealing time at 900 °C for samples A (1×10^{19} B/cm³ B box) and B (2×10^{20} B/cm³ B box) implanted with 20 keV, 10^{14} Si ions/cm². (a) Simulations performed by considering a classical B clustering model are not able to reproduce the evolution of sample B with two different dissolution paths. (b) The inclusion of stable BICs with more than four B atoms in the model (represented as dose of large BICs in the figure) allow us to capture the firstly faster and later slower regimes of dissolution.

while sample B presents two stages in the dissolution, firstly a fast and later a slow dissolution rate. Our model without large BICs reproduces experimental data for sample A. Nonetheless, in the case of sample B simulation results in a lower dose of clustered B than expected and does not predict the slow dissolution rate.

Our extended model for B clustering, including large BICs, allows us to reproduce experimental data for both samples as can be seen in Fig. 1(b). We also include in this figure the dose of low potential energy large BICs formed during annealing of sample B. Note that for sample A the result of the simulation is identical to the one obtained with the model without large BICs (see Fig. 1(a)). Our simulations show that no large BICs are formed in sample A, due to the low B concentration, and thus the decrease of the clustered dose is only controlled by the dissolution of small BICs. In the case of sample B, simulations show that injected Si interstitials during the first step anneal at 815 °C lead to the growth of small BICs, but also a fraction of them evolves into large and more stable BICs (around 44%). During the second step anneal at 900 °C, initially small B clusters start to dissolve by emission of B_i (with an activation energy ~ 3.7 eV) whereas the dose of large BICs remains almost constant. Once small clusters fully dissolve (after ~ 1500 s anneal) the dissolution rate significantly decreases as is only controlled by the emission of B_i from large and more stable BICs.

3. Evolution of BICs in preamorphized Si without the effect of EOR defects

In order to investigate the stoichiometry of BICs resulting after SPER, we have designed an experiment in which B is implanted into preamorphized Si with EOR defects placed far enough from the B profile in order to avoid the interaction between EOR defects and resulting BICs during annealing after SPER. Experiments were performed on n-type, Si Czochralski (100) wafers (resistivity 1.5–4 Ω cm). In order to ensure that EOR defects are far enough from the B profile, reference experiments (not shown in this article) were also performed on a 900 nm-wide, molecular beam epitaxy (MBE) grown, Si film containing a 50 nm-wide $\text{Si}_{1-y}\text{C}_y$ layer ($y=0.3$ at.%) at a depth of 450 nm (which acts as a trap for Si interstitials). Preamorphization implant (PAI) was performed at liquid nitrogen (LN_2) temperature with 500 keV, 5×10^{15} Si^-/cm^2 plus 40 keV, 1×10^{15} Si^-/cm^2 ion beams, obtaining a full amorphous a -layer from the surface down to ~ 950 nm. B implantation at 12 keV, 3×10^{15} B/cm^2 was performed resulting in a B profile with a maximum concentration of 5×10^{20} B/cm^3 at the depth of ~ 60 nm (estimated by SRIM [17]). Implanted B profile and p–n junction are entirely contained within 250 nm from the surface. Then, rapid thermal annealing (RTA) for 60 s at 700 $^\circ\text{C}$ was performed under N_2 flux to induce fully recrystallization of the preamorphized layer. To investigate the electrical B activation as a function of time after SPER, we annealed the samples at 850 or 1000 $^\circ\text{C}$ for times ranging from 1 to 10,000 s. Hall effect was used to determine the Hall active dose (N_H). These measurements are affected by an error of about 5%. The active B dose (N_a) was computed as $N_a = N_H \times r_H$, where r_H is the Hall scattering factor (0.75 for Si [18]).

In order to investigate most probable BIC configurations after SPER, we have compared experimental data with our KMC simulations by considering different initial configurations for BICs transferred into crystalline Si after recrystallization. Because of the

uncertainties in the status resulting after the regrowth we have carried out simplified simulations that can approximate the real case. We have considered the simulated as-implanted B profile as the initial condition for the B profile after SPER, with B concentrations up to 1.9×10^{20} B/cm^3 electrically active to reproduce the experimental initial active B dose (1.6×10^{15} B/cm^2). For higher B concentrations we have considered different B_nI_m configurations, in order to investigate the most predominant configurations that could be transferred into crystalline Si after SPER. Then, we analyze active B evolution during anneals at 850 and 1000 $^\circ\text{C}$ after SPER. Since the evolution of active B takes place in recrystallized Si, we consider the same extended model for BICs discussed in previous section for crystalline Si.

Fig. 2 plots experimental data for the evolution of the active B dose as a function of annealing time at 850 $^\circ\text{C}$ (Fig. 2(a–c)) and at 1000 $^\circ\text{C}$ (Fig. 2(d)) along with our simulation results obtained from different BICs configurations as the starting point for B clusters just after SPER. Experiments indicate that B slowly deactivates during annealing at 850 $^\circ\text{C}$ whereas some reactivation is observed during annealing at 1000 $^\circ\text{C}$. Fig. 2(a) includes simulation results when different B_2I_m configurations are considered. Simulations result in a more accurate fitting when B_2 is considered as the initial condition for B clusters after SPER. Simulations show that this slow B deactivation is mainly controlled by the formation of mobile B_i pairs (through the interaction of equilibrium Si interstitials with active B atoms) that interact with BICs. Thus, main reactions for B deactivation are $\text{B}_2 + \text{B}_i \leftrightarrow \text{B}_3\text{I}$ and $\text{B}_3\text{I} + \text{B}_i \leftrightarrow \text{B}_4\text{I}_2$. The formation rate of B_i is controlled by the transport capability of the equilibrium Si self-interstitial, with a high-activation energy [19] (formation energy + migration energy). Therefore, B deactivation occurs at a slow rate and only a small fraction of B atoms deactivates. However, it is worthy to note that each equilibrium Si interstitial is able to deactivate more than one B atom, since most of BIC configurations with more than one Si intersti-

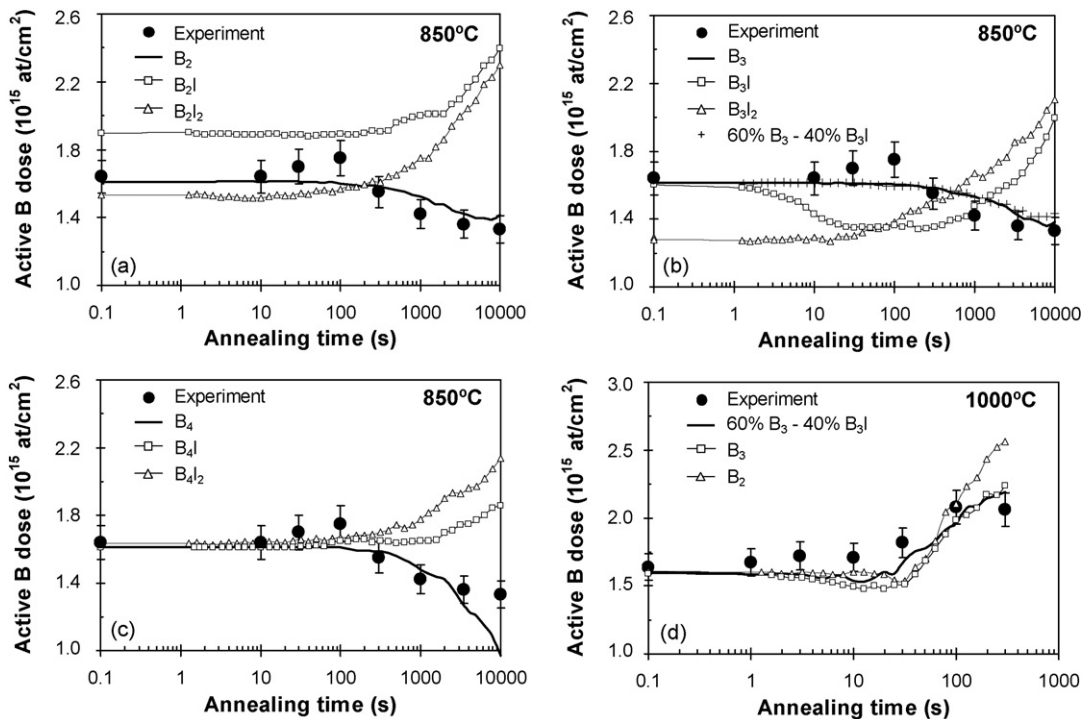


Fig. 2. Evolution of the active B dose as a function of annealing time at (a–c) 850 $^\circ\text{C}$ and (d) 1000 $^\circ\text{C}$ for B implanted at 12 keV, 3×10^{15} B/cm^2 in preamorphized Si with EOR defects placed at a depth ~ 950 nm. Hall measurements data and simulation results with different starting BICs configurations after recrystallization are presented. Best fits are obtained for a mixture of B_3 and B_3I configurations if the percentage of B_3I is lower than 50%.

tial tend to emit Si interstitials quickly (through reactions such as $B_4I_2 \leftrightarrow B_4I+I$), leaving a free Si interstitial that is able to interact with other active B atoms and produce more deactivation reactions. On the contrary, when B_2I and B_2I_2 configurations are considered as starting configurations, simulation results are very far from experiments. Both configurations tend to quickly emit B_i (this occurs for B_2I even during the ramping up of the temperature), since these configurations have low activation energy for the emission of B_i in the model, according to theoretical calculations. Then, although a fraction of B clusters grow into B_3I and B_4I configurations, the net effect is B reactivation as B cluster growth is not very favored.

Fig. 2(b) include simulation data for different B_3I_m configurations as the starting point for BICs. Similarly to B_2 , simulations also show a more accurate fitting when B_3 is considered as the initial configuration. Deactivation also occurs due to thermally generated Si interstitials, although in this situation the simulation shows some evolution of B clusters towards large BICs. Nevertheless, as the amount of Si interstitials in B_3I_m configurations increases, faster deactivation is observed (even during the ramping up to the temperature in the case of B_3I_2) and subsequent reactivation occurs sooner. It is worthy to note that the simulated time evolution at 850 °C practically does not change if we consider as initial conditions a mixture of B_3 and B_3I configurations when the percentage of B_3I is maintained below 50% (i.e. 40% B_3I and 60% B_3 in Fig. 2(b)). Higher percentages of B_3I result in a progressively faster deactivation than expected. This acceleration of B deactivation could be explained as follows. When all initial BICs are in the configuration B_3 , the most probable reactions will be $B_3+I \leftrightarrow B_3I$ which has low potential energy in the model, or $B_3+B_i \leftrightarrow B_4I$, also with low potential energy in the model. Thus, deactivation reactions are controlled by thermally generated Si interstitials. However, when all initial BICs are in the configuration B_3I , the possible reactions will be $B_3I+I \leftrightarrow B_3I_2 \leftrightarrow B_3I+I$ and $B_3I+B_i \leftrightarrow B_4I_2 \leftrightarrow B_4I+I$, which tend to emit a Si interstitial quickly to reach B_3I and B_4I configurations. Thus, once equilibrium Si interstitials start deactivation reactions, extra Si interstitials contained in the initial BICs will be liberated and available to interact with other BICs. These extra Si interstitials, contained initially in the starting configurations of BICs, accelerates the deactivation process.

Simulation results for B_4I_m initial configurations are plotted in Fig. 2(c), showing more severe deactivation for B_4 than the experimentally observed. Since B concentration is high, the thermally generated Si interstitials lead to the evolution of a fraction of B_4 into larger and more stable configurations such as B_6I , B_7I , etc. Concerning to B_4I and B_4I_2 configurations, also some B clusters grow into large BICs, but Si interstitials favor also dissolution as discussed above, resulting in B reactivation as a net effect. Note that in the case of B_4I_m configurations the presence Si interstitials does not accelerate deactivation as occur for B_3I_m configurations, since the evolution towards large BICs is energetically not very favorable in our model. It is worthy to note that independently on the number of B atoms in the initial BICs configurations, simulations indicate that initial BICs should not content a large amount of Si interstitials since they lead to an excessive broadening of B profiles by diffusion. This observation is also in agreement with reported theoretical calculations that obtains BICs with low content of Si interstitials after SPER [12], although those authors did not predict the formation of B clusters with only substitutional B atoms (such as B_2 or B_3). However, our simulations suggest that starting conditions with all BICs containing at least one Si interstitial atom lead to more B deactivation and more B diffusion than expected. Although some of the proposed configurations (B_2 and B_3) are very unsta-

ble in the model, their formation during recrystallization could be energetically favorable since recrystallization removes Si interstitials and the formation of configurations with Si interstitials (such as B_2I , B_3I , etc.) could require the formation of an extra Si interstitial [15].

Finally, we have analyzed the evolution of active B dose during annealing at 1000 °C. In Fig. 2(d) we consider initial B cluster configurations that resulted in a better fitting between simulations and experimental data at 850 °C. We obtain better results for B_3 or even for a mixture of 60% B_3 and 40% B_3I , while B_2 lead to faster reactivation. The slightly better results obtained by BICs configurations with three B atoms compared to configurations with two B atoms is associated to the formation of more stable large BICs in the first case that slightly slow down B reactivation.

4. Conclusions

An extended model for B clustering that includes larger and more stable configurations than classical models has been developed to account for BICs dissolution kinetics in crystalline Si under conditions below and above s.l. At low B concentrations B dissolution takes place by emission of mobile B_i by usual small BICs. However, at very high B concentrations, a fraction of small BICs are able to evolve to larger and more stable configurations that coexist with small BICs. Under these conditions smaller and less stable clusters dissolve faster, leading to a initial dissolution stage with faster dissolution rate. Once smaller BICs disappear, B dissolution is controlled by the emission of B_i from larger and more stable BICs, resulting in a second dissolution stage much slower.

Experimental data complemented with a detailed simulation study on B activation in preamorphized Si avoiding the influence of EOR defects have been presented, in order to investigate the stoichiometry of BICs obtained after SPER. This analysis indicates that initial BICs after recrystallization should not contain a high amount of Si interstitials. Otherwise, B deactivation and subsequent reactivation that takes place during subsequent anneals after SPER will occur faster than experimentally observed. Simulations suggest B_3 and B_3I clusters are probably the most predominant configurations resulting after recrystallization.

Acknowledgment

This work has been supported by the Spanish DGI under project TEC2005-05101.

References

- [1] S.C. Jain, W. Schoenmaker, R. Lindsay, P.A. Stolk, S. Decoutere, M. Willander, H.E. Maes, *J. Appl. Phys.* 91 (2002) 8919 (and references therein).
- [2] S. Solmi, F. Baruffaldi, R. Canteri, *J. Appl. Phys.* 69 (1991) 2135.
- [3] M.J. Caturla, M.D. Johnson, T. Diaz de la Rubia, *Appl. Phys. Lett.* 72 (1998) 2736.
- [4] X.-Y. Liu, W. Windl, Michael P. Masquelier, *Appl. Phys. Lett.* 77 (2000) 2018.
- [5] P. Alippi, P. Ruggerone, L. Colombo, *Phys. Rev. B* 69 (2004) 125205.
- [6] L. Pelaz, G.H. Gilmer, H.-J. Gossmann, J.M. Poate, C.S. Rafferty, M. Jaraiz, J. Barbolla, *Appl. Phys. Lett.* 74 (1999) 3657.
- [7] M. Aboy, L. Pelaz, L.A. Marqués, P. López, J. Barbolla, *J. Appl. Phys.* 97 (2005) 103520 (and references therein).
- [8] F. Cristiano, X. Hebras, N. Cherkashin, A. Claverie, W. Lerch, S. Paul, *Appl. Phys. Lett.* 83 (2005) 5407.
- [9] S. Boninelli, S. Mirabella, E. Bruno, F. Priolo, F. Cristiano, A. Claverie, D. De Salvador, G. Bisognin, E. Napolitani, *Appl. Phys. Lett.* 91 (2007) 031905.
- [10] D. De Salvador, E. Napolitani, G. Bisognin, A. Carnera, E. Bruno, S. Mirabella, G. Impellizzeri, F. Priolo, *Mater. Sci. Eng. B* 124–125 (2005) 32.
- [11] J.-Y. Jin, J. Liu, U. Jeong, S. Mehta, K. Jones, *J. Vac. Sci. Technol. B* 20 (2002) 422.
- [12] A. Mattoni, L. Colombo, *Phys. Rev. B* 69 (2004) 045204.
- [13] M. Jaraiz, L. Pelaz, E. Rubio, J. Barbolla, G.H. Gilmer, D.J. Eaglesham, H.J. Gossmann, J.M. Poate, *Mater. Res. Soc. Symp. Proc.* 532 (1998) 43.

- [14] L. Pelaz, L.A. Marqués, M. Aboy, P. López, J. Barbolla, *Comput. Mater. Sci.* 33 (2005) 92.
- [15] L. Pelaz, M. Aboy, P. López, L.A. Marqués, I. Santos, *Nucl. Instrum. Methods B* 253 (2006) 41.
- [16] A. Armigliato, D. Nobili, P. Ostojja, M. Servidori, S. Solmi, in: H. Huff, E. Sirtl (Eds.), *Semiconductor Silicon 1977*, vol. 77, no. 2, The Electrochemical Society, Princeton, NJ, 1977, p. 638.
- [17] J.F. Ziegler, J.P. Biersack, U. Littmark, *The Stopping and Range of Ions in Solids*, vol. 1 of Series *Stopping and Ranges of Ions in Matter*, Pergamon Press, New York, 1984, www.srim.org.
- [18] L. Romano, E. Napolitani, V. Privitera, S. Scalese, A. Terrasi, S. Mirabella, M.G. Grimaldi, *Mater. Sci. Eng. B* 102 (2003) 49.
- [19] H. Bracht, E.E. Haller, R. Clark-Phelps, *Phys. Rev. Lett.* 81 (1998) 393.